

RESEARCH ARTICLE

10.1029/2017JD028063

Key Points:

- In the 900-cm<sup>-1</sup> atmospheric window channel several Radiative Transfer Models have a better than 0.95 correlation between the histogram derived from the observations and those derived from the calculations
- Differences in the bias between observations and calculations for the 2,616-cm<sup>-1</sup> atmospheric window channel are not inconsistent with results at 900 cm<sup>-1</sup> if the daytime calculations use full scattering
- Differences in the cloud physics and cloud overlap assumptions between Radiative Transfer Models result in a standard deviation of the pairwise difference of between 6 and 12 K; differences due to the cloud overlap assumption alone result in a 3-K standard deviation

Correspondence to:

H. H. Aumann, [aumann@jpl.nasa.gov](mailto:aumann@jpl.nasa.gov)

Citation:

Aumann, H. H., Chen, X., Fishbein, E., Geer, A., Havemann, S., Huang, X., et al. (2018). Evaluation of radiative transfer models with clouds. *Journal of Geophysical Research: Atmospheres*, 123, 6142–6157. <https://doi.org/10.1029/2017JD028063>

Received 14 NOV 2017

Accepted 4 APR 2018

Accepted article online 16 APR 2018

Published online 13 JUN 2018

Evaluation of Radiative Transfer Models With Clouds

Hartmut H. Aumann<sup>1</sup>, Xihong Chen<sup>2</sup>, Evan Fishbein<sup>1</sup>, Alan Geer<sup>3</sup>, Stephan Havemann<sup>4</sup>, Xianglei Huang<sup>2</sup>, Xu Liu<sup>5</sup>, Giuliano Liuzzi<sup>6</sup>, Sergio DeSouza-Machado<sup>7</sup>, Evan M. Manning<sup>1</sup>, Guido Masiello<sup>6</sup>, Marco Matricardi<sup>3</sup>, Isaac Moradi<sup>8</sup>, Vijay Natraj<sup>1</sup>, Carmine Serio<sup>6</sup>, Larrabee Strow<sup>7</sup>, Jerome Vidot<sup>9</sup>, R. Chris Wilson<sup>1</sup>, Wan Wu<sup>5</sup>, Qiguang Yang<sup>5</sup>, and Yuk L. Yung<sup>1,10</sup>

<sup>1</sup>Jet Propulsion Laboratory, California Institute of Technology, Pasadena, CA, USA, <sup>2</sup>Department of Climate and Space Science, University of Michigan, Ann Arbor, MI, USA, <sup>3</sup>European Center for Medium-Range Weather Forecasting, Reading, UK, <sup>4</sup>UK Met Office, Exeter, UK, <sup>5</sup>NASA Langley Research Center, Hampton, VA, USA, <sup>6</sup>School of Engineering, University of Basilicata, Potenza, Italy, <sup>7</sup>Department of Physics, University of Maryland, Baltimore County, Catonsville, MD, USA, <sup>8</sup>ESSIC, University of Maryland, College Park, MD, USA, <sup>9</sup>Meteo France, Toulouse, France, <sup>10</sup>Department of Planetary Science, California Institute of Technology, Pasadena, CA, USA

**Abstract** Data from hyperspectral infrared sounders are routinely ingested worldwide by the National Weather Centers. The cloud-free fraction of this data is used for initializing forecasts which include temperature, water vapor, water cloud, and ice cloud profiles on a global grid. Although the data from these sounders are sensitive to the vertical distribution of ice and liquid water in clouds, this information is not fully utilized. In the future, this information could be used for validating clouds in National Weather Center models and for initializing forecasts. We evaluate how well the calculated radiances from hyperspectral Radiative Transfer Models (RTMs) compare to cloudy radiances observed by AIRS and to one another. Vertical profiles of the clouds, temperature, and water vapor from the European Center for Medium-Range Weather Forecasting were used as input for the RTMs. For nonfrozen ocean day and night data, the histograms derived from the calculations by several RTMs at 900 cm<sup>-1</sup> have a better than 0.95 correlation with the histogram derived from the AIRS observations, with a bias relative to AIRS of typically less than 2 K. Differences in the cloud physics and cloud overlap assumptions result in little bias between the RTMs, but the standard deviation of the differences ranges from 6 to 12 K. Results at 2,616 cm<sup>-1</sup> at night are reasonably consistent with results at 900 cm<sup>-1</sup>. Except for RTMs which use full scattering calculations, the bias and histogram correlations at 2,616 cm<sup>-1</sup> are inferior to those at 900 cm<sup>-1</sup> for daytime calculations.

**Plain Language Summary** Getting the right clouds of the right type, at the right time and location in Global Circulation Models, is key to getting the local energy balance right. This is key to an accurate forecast. If the clouds are of the wrong type or at the wrong location or time, the accuracy of the forecast is degraded. We evaluate the accuracy of the best currently available cloud description (produced by the European Center for Medium-Range Weather Forecasting) by comparing the radiances calculated using Radiative Transfer Models (RTMs) from six major development teams to cloudy radiances observed by the Atmospheric Infrared Sounder at the same location and time. The better RTMs fit statistically reasonably well in the 11-μm atmospheric window area, with little latitude (zonal) and day/night cloud-type related bias. None of the RTMs fit well in the 4-μm atmospheric window area during daytime, unless the calculations use full scattering. With the current state of art, all major RTMs would be suitable to start the validation of cloud effects in the National Weather Center models using just one 11-μm atmospheric window channel.

1. Introduction

Clouds are a key component of the Earth’s weather and climate system. The data from hyperspectral infrared sounders have the information content to sense the vertical distribution of temperature and water vapor in clear air and of ice and liquid water inside semitransparent clouds. The data from four hyperspectral sounders in polar orbit are routinely ingested by the National Weather Centers (NWCs; e.g., Collard & McNally, 2009): The Atmospheric Infrared Sounder (AIRS; Aumann et al., 2003) on the Earth Observing System Aqua satellite, the Crosstrack Infrared Sounder (CrIS, Glumb et al., 2003) on the Suomi National Polar-orbiting Platform satellite, and the Infrared Atmospheric Sounder Interferometer (IASI, Blumstein et al., 2008; Hilton et al., 2012) on MetOp A and B each makes more than 2 million observations of the state of the atmosphere and the clouds each day. The NWCs predominantly use the cloud-free portion of these data to initialize forecasts that

**Table 1**  
*Cloudy RTM Developers Who Participated in the Comparison*

RTM name	Base model spectroscopy	Participant	Organization
SARTA	HITRAN2008	DeSouza-Machado Strow	UMBC
RTTOV	HITRAN2008	Vidot Matricardi	NWPSAF (France) ECMWF (EU)
HT-FRTC	HITRAN2008	Havemann	UK Met Office
PCRTM	HITRAN2008	Xianglei Huang	University of Michigan
CRTM	HITRAN2008	Xu Liu	LARC
		Moradi, Wilson	NASA GMAO NASA JPL
$\sigma$ -IASI-as	HITRAN2012	Liuzzi Masiello	U. Basilicata, Italy

provide temperature, water vapor, water cloud, and ice cloud profiles on a global grid every 3 hr. Using cloudy observations in forecast models is difficult (Bennartz & Greenwald, 2011; Errico et al., 2007; McNally, 2009; McNally & Watts, 2003; Okamoto et al., 2014; Pavelin et al., 2008), and although all-sky microwave radiances are now used (e.g., Geer et al., 2017), the use of infrared radiances represents a harder problem. NWCs make use of some cloudy scenes, such as low-level cloud or fully overcast scenes, but the cloud information is still not used to initialize forecasts (Guidard et al., 2011; Lavanant et al., 2011). A number of NWCs and university research groups have developed fast and accurate Radiative Transfer Models (RTMs) for infrared sounders, which include the effects of cloud and aerosol scattering. The names and associated organizations of the RTM developers are summarized in Table 1.

Summaries of the RTMs are found in Appendix A3. While each RTM has been subject to its own validation, our paper is the first to compare results from major RTMs for cloudy hyperspectral infrared applications on the same data set to collocated observations and to each other.

The objective of our paper was to evaluate the degree to which the radiative effects of clouds in NWC models agree with collocated hyperspectral observation. The availability of RTMs with a high degree of radiometric fidelity relative to observation, or at least the availability of tools to assess this fidelity, is expected to lead to the increased utilization of hyperspectral sounder data in the forecast. We selected AIRS observations and AIRS RTMs for our analysis to follow the Saunders et al. (2007) RTM analysis under cloud-free conditions.

## 2. Data, Participants, and Evaluation

### 2.1. Data

We selected data provided by the European Center for Medium-Range Weather Forecasting (ECMWF; European Center for Medium-Range Weather Forecasting (ECMWF), 2009) as representative for the definition of the atmospheric states with clouds. The ECMWF description of the atmospheric state (temperature, water vapor and cloud vertical profiles, and surface temperature) has been widely documented and validated (e.g., Kazumori et al., 2016; Köhler et al., 2011; Tiedtke, 1989, 1993; Tompkins et al., 2007). Details are in Appendix A1.

For the intercomparison of RTMs we used AIRS observations from 1 March 2009 and the matching atmospheric state defined by ECMWF. A subset of this data was created using the difference between the ECMWF estimate of the surface temperature (stemp) and the brightness temperature measured in the  $1,231\text{-cm}^{-1}$  window channel (bt1231; stemp-bt1231). This difference is a measure of the radiometric effect of clouds. Under clear conditions the difference is less than 2 K, but the difference can increase to as much as 100 K in the presence of cold clouds in the tropics. We limited the size of this data set to control the magnitude of the computational effort involved in scattering calculations by using stratified sampling. This method selected a representative mix of cloudy conditions from the AIRS data, which resulted in 7,377 unique cases. The surface emissivity and surface reflectance were obtained from a monthly climatology (Zhou et al., 2012). The surface reflectance was assumed to be Lambertian. Details of the selection algorithm are given in Appendix A2.

### 2.2. Participants and RTM Methodology

Table 1 summarizes the affiliation of the developers of cloud-capable RTMs at major NWCs, government, and university facilities. Six RTMs were used: (1) Stand Alone Radiative Transfer Algorithm (SARTA), (2) Radiative Transfer for TOVS (RTTOV), (3) Havemann-Taylor Fast Radiative Transfer Code (HT-FRTC), (4) Principal Component-based RTM (PCRTM), (5) Community RTM (CRTM), and (6)  $\sigma$ -IASI. Largely based on discussions at the 2016 AGU meeting, every RTM team, except the RTTOV teams, submitted revised results. Five of the RTM developers generated variants related to details of how cloud overlap, cloud type, and scattering were handled. Details on the individual RTMs are summarized in Appendix A3.

All RTMs calculated cloudy radiances using a linear combination of clear-sky calculations and scattering calculations for one or more cloud columns. The results of the clear-sky column calculations from all these RTMs

were nearly identical, consistent with Saunders et al. (2007). The cloudy spectra were calculated as the linear combination of clear and cloudy columns based on the cloud fraction. The maximum overlap (MO) model is the simplest case:

$$R_{MO} = CF R_{FO} + (1 - CF) R_{CLR} \quad (1)$$

$R_{MO}$  is the spectrum calculated with the MO assumption and CF is defined as the maximum cloud fraction in the cloud coverage profile. Some RTMs set CF equal to the total cloud cover (tcc) specified in the ECMWF record.  $R_{CLR}$  is the clear-sky spectrum, and  $R_{FO}$  is the spectrum assuming full overcast (i.e., clouds fill the entire satellite footprint). Some RTMs allow the user to make more complicated overlap assumptions. The maximum random overlap (MRO) assumption states that any continuous vertical cloud profile is maximally overlapped, and the discontinuous parts of the vertical cloud profile are randomly overlapped (Hogan & Illingworth, 2000). If two cloud slabs are used, the MRO radiance is

$$R_{MRO} = CF_1 (1 - CF_2) R_{C1} + CF_2 (1 - CF_1) R_{C2} + CF_1 CF_2 R_{CLD} + (1 - CF_1) (1 - CF_2) R_{CLR} \quad (2)$$

where  $CF_1$  is the maximum cloud fraction of the first cloud slab,  $CF_2$  is the maximum cloud fraction of the second cloud slab,  $R_{C1}$  is the calculation where only the first cloud slab is included,  $R_{C2}$  is the calculation where only the second cloud slab is included,  $R_{CLD}$  is the calculation where both clouds are included, and  $R_{CLR}$  is the clear-sky calculation. There are several variants of the overlap assumption, including MO, exponential random overlap (ERO), and the random overlap (RO). We indicated these variants in the names of the models; for example, CRTM\_mro is the cloudy spectrum calculated using CRTM with the MRO assumption. Most RTM developers submitted results with a number of variants.

### 2.3. Evaluation

The intercomparison of the RTMs used three methods.

1. The pairwise comparison of the observed AIRS spectra with the calculated spectra. We calculated the mean and standard deviation (stddev). This comparison is complicated by several factors: (a) The collocation error: The location and local time of the AIRS data obtained with a 12-km footprint (effectively 1/8 degree latitude/longitude in the tropics) is not a good match to the temporal (3 hr) and spatial grid (approximately 25 km) of the ECMWF data available to this study. (b) The tcc is specified in the ECMWF data; the cloud fraction, liquid water, and ice water content are specified for each level, but the cloud overlap is not specified. Each RTM can handle the cloud overlap with different assumptions. (c) The ECMWF description of the cloud in 91 levels is itself subject to random and systematic errors. (d) The liquid water and ice cloud particle size distributions are not directly specified. For a sufficiently large data set, factor (a) should have zero bias but will cause a large stddev. Factors (b), (c), and (d) may create a bias as well as a large stddev.
2. Characterization of the radiometric effect of clouds using histograms of (stemp-bt). Here stemp is the surface temperature from ECMWF and bt is the AIRS observed or RTM-calculated brightness temperature in an atmospheric window channel. In the absence of a solar reflected component, (stemp-bt) increases from near zero under clear conditions to 100 K with increasing cloudiness. Under ideal conditions of a perfect matchup between AIRS and ECMWF, perfect clouds and thermodynamic profiles in the ECMWF model, and a perfect RTM, the two histograms will be identical. We evaluate the closeness of the match between observations and calculations by calculating the histogram correlation. Small residual biases that result from compensatory large positive and negative differences between AIRS and the RTM calculations under different conditions of cloudiness (or cloud types) are revealed as distortions of the histograms, resulting in a lowered correlation with the observations. This approach is not sensitive to random errors in the ECMWF cloud forecasts (e.g., the miss-location of clouds) but remains vulnerable to systematic errors; nevertheless, known systematic errors in ECMWF cloud forecasts are globally infrequent and limited to specific meteorological conditions (Kazumori et al., 2016). Infrequent ECMWF cloud errors are not likely to impact the histogram correlation because of the wide variety of cloud conditions in our data set.
3. The pairwise comparison of results from different RTMs. This approach has the advantage that it sidesteps matchup uncertainties with ECMWF. All RTMs use the same cloud model description. The comparison reveals the radiometric effect of differences between RTMs in cloud microphysics assumptions, cloud overlap assumptions, and scattering algorithms.

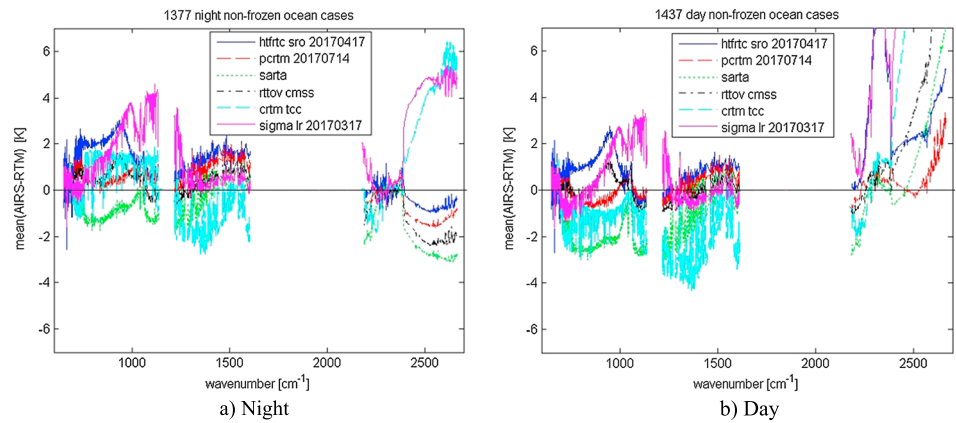
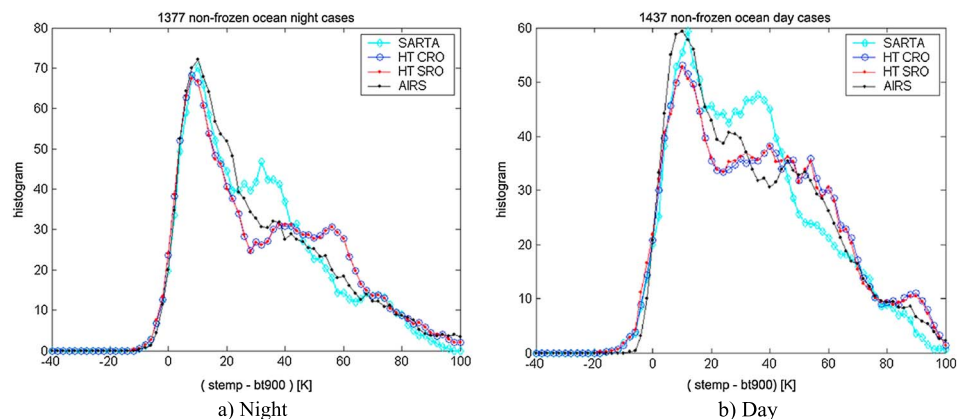


**Figure 1.** (a, b) Mean difference between Atmospheric Infrared Sounder (AIRS) and six Radiative Transfer Model (RTM) implementations for nonfrozen ocean cases.

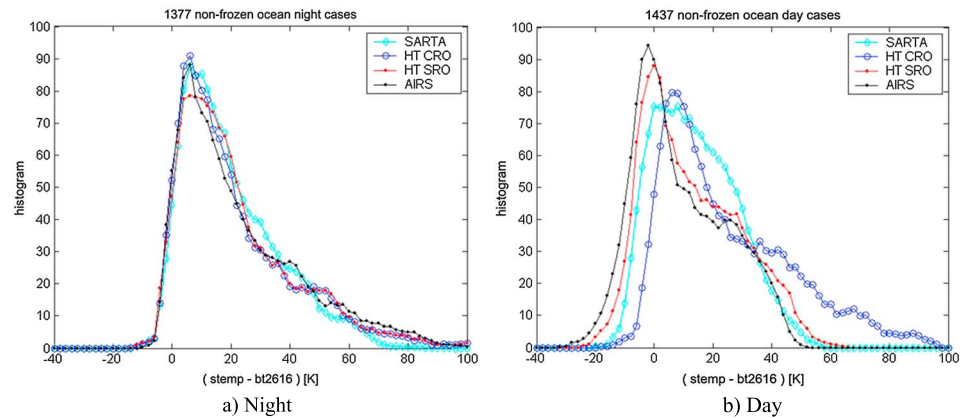
### 3. Results

Figure 1 illustrates typical spectral patterns in the mean of the pairwise difference between AIRS spectra and the spectra calculated using six representative RTMs for 1,377 night and 1,437 day nonfrozen ocean cases, respectively. For wavenumbers lower than  $1,700 \text{ cm}^{-1}$  there is a relatively day/night independent, spectrally correlated pattern in the mean of the difference between AIRS and different RTMs. For wavenumbers above  $2,200 \text{ cm}^{-1}$  the pattern for the different RTMs is inconsistent even for the nighttime data. This inconsistency is even larger for the daytime data due to the differences in the way the RTMs deal with scattering and solar-reflected radiation. For the detailed evaluation of the RTMs we focus on the two representative atmospheric window channels at  $900$  and  $2,616 \text{ cm}^{-1}$ .

Figure 2 illustrates the comparison between AIRS and three RTMs at  $900 \text{ cm}^{-1}$  for the same two cases as Figure 1 using histograms of  $(\text{stemp}-\text{bt}900)$ . The peak of the histogram in all cases is near  $+10 \text{ K}$ , that is, relatively little cloudiness or low clouds. The coldest cloud tops are  $100 \text{ K}$  colder than  $\text{stemp}$ . The black trace is derived from the AIRS observation. HT\_CRO and HT\_SRO results are nearly identical, even though HT\_CRO uses Chou scaling, while HT\_SRO uses a full scattering calculation (both RTMs use the RO assumption). SARTA traced the AIRS histogram somewhat better than either HT variant for nighttime cases with  $(\text{stemp}-\text{bt}900)$  between  $40$  and  $70 \text{ K}$ , with SARTA finding many more cases than AIRS, while the HT RTMs had less cases. SARTA uses Chou scaling and the RO assumption similar to HT\_CRO. However, SARTA takes multileveled clouds and converts them into two single layer clouds, one for ice clouds and one for water clouds.



**Figure 2.** (a, b) Histograms for  $(\text{stemp}-\text{bt}900)$  observed by Atmospheric Infrared Sounder (AIRS) and calculated by three representative Radiative Transfer Models.



**Figure 3.** (a, b) Histograms for stemp-bt2616 observed by Atmospheric Infrared Sounder (AIRS) and calculated by three representative Radiative Transfer Models.

For daytime cases (Figure 2b), both SARTA and HT RTMs deviated from the AIRS trace for (stemp-bt900) cases between 15 and 70 K. Similar to the nighttime case, SARTA had more cases than AIRS in this range, while both versions of HT had less cases than AIRS between 15 and 30 K.

Figure 3 illustrates the histogram comparison using the same three RTMs and the same day and night non-frozen ocean cases as Figure 2 but at  $2,616\text{ cm}^{-1}$ . In this figure the agreement between the RTMs and AIRS at night is much better than during the day. In fact, the histograms from SARTA and both HT RTMs are more closely matched to the AIRS histogram for cases between 15 and 70 K than the histograms at  $900\text{ cm}^{-1}$  (Figure 2a). During the day the full scattering calculations used by HT\_SRO result in histograms without the long tail for high clouds (stemp-bt2616 > 60 K) seen in the HT\_CRO histogram.

### 3.1. Numerical Summary of Histogram Correlations, Bias, and Standard Deviations

Table 2 summarizes the histogram correlations and the bias relative to AIRS for the day and night nonfrozen ocean cases at  $900\text{ cm}^{-1}$ . The results shown are separated into six groups, with each group representing the

**Table 2**  
Histogram Correlation and Bias for Day and Night Nonfrozen Ocean Cases at  $900\text{ cm}^{-1}$

AIRS-bt900	Day correlation	Day bias $\pm$ stddev (K) 1,437 cases	Night correlation	Night bias $\pm$ stddev (K) 1,377 cases	Day-night bias (K)
SARTA_TwoSlab(C)	0.9502	-2.33 $\pm$ 22.1	0.9707	-0.96 $\pm$ 19.5	-1.3
SARTA_TwoSlab(P)	0.9621	+2.23 $\pm$ 22.9	0.9710	+2.80 $\pm$ 20.4	-0.6
PCRTM_ERO	0.9629	+0.53 $\pm$ 21.5	0.9792	+1.37 $\pm$ 19.5	-0.8
PCRTM_MRO	0.9591	-0.21 $\pm$ 21.1	0.9796	-0.36 $\pm$ 19.1	-0.5
PCRTM_ERO2	0.9680	+0.96 $\pm$ 22.8	0.9785	+1.37 $\pm$ 21.1	-0.5
PCRTM_MRO4	0.9715	-0.53 $\pm$ 22.36	0.9625	+0.38 $\pm$ 19.85	-0.8
HT_CMO	0.9773	+1.09 $\pm$ 22.58	0.9591	+1.12 $\pm$ 20.36	-0.0
HT_CRO	0.9695	+2.18 $\pm$ 22.26	0.9638	+2.53 $\pm$ 20.04	-0.3
HT_CMRO	0.9774	+1.15 $\pm$ 22.56	0.9613	+1.26 $\pm$ 20.29	-0.1
HT_SMRO	0.9764	+0.60 $\pm$ 22.54	0.9591	+1.12 $\pm$ 20.36	-0.5
HT_SRO	0.9692	+1.69 $\pm$ 22.22	0.9629	+2.47 $\pm$ 20.07	-0.7
HT_SMRO	0.9765	+0.67 $\pm$ 22.52	0.9590	+1.18 $\pm$ 20.34	-0.5
RTTOV_MRO	0.9666	-4.22 $\pm$ 21.42	0.9748	-3.65 $\pm$ 19.5	-0.8
RTTOV_CMSS	0.9107	+0.69 $\pm$ 21.62	0.9105	+1.04 $\pm$ 20.0	-0.4
$\sigma$ -IASI	0.9261	+0.75 $\pm$ 20.9	0.9437	+2.02 $\pm$ 19.2	-1.3
CRTM_tcc	0.8816	-0.98 $\pm$ 21.1	0.8915	+1.46 $\pm$ 19.97	-0.5
CRTM_mro	0.9552	-0.72 $\pm$ 23.9	0.9819	-0.10 $\pm$ 20.8	-0.6
CRTM_2col	0.9553	+0.12 $\pm$ 23.9	0.9817	+0.71 $\pm$ 21.3	-0.6
Clear column RTM (SARTA)	0.4168	-29.57 $\pm$ 22.8	0.4631	-25.78 $\pm$ 22.1	+3.8
Corr > 0.9		17 of 18		17 of 18	
mean bias		+0.3		+0.8	
mean stddev		22		20	



**Table 3**

*Bias and Standard Deviation of bt900 Calculated for 1,437 Day Nonfrozen Ocean Cases Relative to CRTM\_mro, HT\_SMRO, PCRTM\_MRO4, and RTTOV\_MRO*

bt900 (RTM-reference)	Reference CRTM_mro bias ± stddev (K)	Reference HT_SMRO bias ± stddev (K)	Reference PCRTM_MRO4 bias ± stddev (K)	Reference RTTOV_MRO bias ± stddev (K)
SARTA TwoSlab(C) pnewM1 pnewM1	+1.69 ± 12.10	2.99 ± 11.79	+1.79 ± 10.52	−1.90 ± 11.63
SARTA TwoSlab(P) pnew999	−2.72 ± 11.32	−1.58 ± 10.69	−2.75 ± 9.76	−6.47 ± 10.79
PCRTM_ERO	−1.28 ± 9.90	+0.12 ± 6.83	−1.00 ± 6.39	−4.78 ± 6.59
PCRTM_MRO	−0.32 ± 13.89	1.22 ± 9.60	−0.06 ± 9.80	−3.65 ± 9.47
PCRTM_ERO2	−1.28 ± 12.58	−0.06 ± 9.69	−1.27 ± 9.46	−4.94 ± 9.64
PCRTM_MRO4	−0.13 ± 11.44	+1.26 ± 7.57	0.00 ± 0.00	+3.59 ± 7.51
HT_CMO	−1.65 ± 12.54	−0.43 ± 0.39	−1.68 ± 7.69	−5.31 ± 5.72
HT_CRO	−2.75 ± 12.19	−1.40 ± 1.79	−2.74 ± 7.44	−6.41 ± 5.87
HT_CMRO	−1.72 ± 12.55	−0.48 ± 0.35	−1.75 ± 7.69	−5.38 ± 5.73
HT_SMO	−1.17 ± 12.41	+0.04 ± 0.17	−1.20 ± 7.58	−4.83 ± 5.57
HT_SRO	−2.25 ± 12.08	−0.91 ± 1.82	−2.25 ± 7.35	−5.91 ± 5.74
HT_SMRO	−1.24 ± 12.42	0.00 ± 0.00	−1.26 ± 7.57	−4.90 ± 5.57
RTTOV_MRO	+3.65 ± 12.70	+4.90 ± 5.57	+3.59 ± 7.51	0.00 ± 0.00
RTTOV_CMSS	−1.34 ± 10.35	−0.02 ± 5.62	−1.23 ± 6.93	−4.92 ± 6.45
σ-IASI-As	−1.49 ± 12.85	−0.10 ± 6.85	−1.37 ± 7.99	−5.00 ± 4.34
CRTM_tcc	+0.20 ± 14.02	+1.64 ± 14.07	+0.43 ± 11.86	−3.26 ± 10.57
CRTM_mro	0.00 ± 0.00	+1.24 ± 12.42	+0.13 ± 11.44	−3.65 ± 12.70
CRTM_2col	−0.60 ± 3.43	+0.47 ± 12.22	+0.65 ± 11.22	−4.29 ± 12.75
Five-group bias	−0.2	+1.5	+0.3	−3.4
Five-group stddev	12.3	7.6	8.7	6.5

six RTM developers. The histogram correlations with AIRS exceeded 0.95 for five of the six groups for day and night cases. The histogram correlations were slightly higher for the night cases than for the day cases. This observation may be related to a day/night dependence of the cloud structure or microphysics properties. A more in-depth study of his observation is beyond the scope of this paper. The row labeled “clear column RTM” used SARTA without clouds. The mean bias relative to AIRS for all RTMs was +0.3 K (range − 4.2 K to +2.2 K) for the day cases, and + 0.8 K (range − 3.6 K to +2.8 K) for the night cases. The number following the plus-minus symbol in Table 2 is the stddev of the differences, typically 22 K for the day and 20 K for the night cases. Using the typical stddev for nighttime, the probable error in the mean is about  $22/\sqrt{1377} = 0.6$  K (assuming random sampling and uncorrelated errors). Bias differences of more than three times the probable error, 2 K, are significant.

When the RTM calculations are compared to one another, the effect of the collocation error is eliminated, since we are comparing calculations for the same cloud conditions. Results are shown in Table 3 for the 1,437 day nonfrozen ocean cases using four RTMs as references: CRTM\_mro, HT\_SMRO, PCRTM\_MRO4, and RTTOV\_MRO. For the “five-group” summary in the last row we used only the first entry from each group, excluding the RTM used as the reference. The bias between RTMs was −0.2, +1.5, +0.3, and − 3.4 K, and the stddevs were 12.3, 7.6, 8.7, and 6.5 K, respectively, for the four reference RTMs.

In order to explore the extent to which a small bias on a global scale may be the result of compensating biases, we divided the data into latitude zones. Results are summarized in Table 4 for the tropical zone ( $|\text{lat}| < 30^\circ$ ) with 3,644 cases; 2,662 cases for the extratropical zone ( $|\text{lat}| > 30^\circ$ ), limited to nonfrozen surface cases using stemp >275 K; and 1,070 cases from the polar zone ( $|\text{lat}| > 60^\circ$ ). Based on the last column in Table 4, which shows the difference between the mean tropical and the mean midlatitude bias, some RTMs show a latitude dependence in the bias of several degree kelvin.

Table 5 summarizes the results at  $2,616 \text{ cm}^{-1}$  for day and night nonfrozen ocean. The bottom row summarizes the results in terms of a mean bias and stddev, excluding RTMs with less than 0.9 histogram correlation with AIRS. At night 16 of the 18 RTMs had a mean bias relative to AIRS of −1.8 K with 20 K stddev and five of the six RTM teams produced results with histogram correlation with AIRS better than 0.95. During the day only two of the six RTM teams produced results with histogram correlations with AIRS better than 0.95. For these cases the mean bias was +2.4 K, and the mean stddev was 16 K.

**Table 4**

*Bias and Standard Deviation Between AIRS bt900 and Different RTMs Separated Into the Tropical, Midlatitude, and Polar Zones (as Defined in the Text)*

bt900 (AIRS observed—calculated; K)	Tropical zone 3,644 cases bias ± stddev (K)	Mid latitude 2,662 cases bias ± stddev (K)	Polar 1,070 cases bias ± stddev (K)	Tropical—midlatitude bias (K)
SARTA TwoSlab(C)	+0.41 ± 22.59	−4.66 ± 14.84	+3.19 ± 10.15	+5.0
SARTA TwoSlab(P)	+4.15 ± 23.51	−2.57 ± 15.02	+0.79 ± 10.06	+6.7
PCRTM_ERO	+2.63 ± 22.48	−2.86 ± 13.86	−0.53 ± 9.60	+5.5
PCRTM_MRO	+0.35 ± 22.01	−3.42 ± 13.93	−0.56 ± 9.63	+3.8
PCRTM_ERO2	+3.21 ± 24.33	−2.65 ± 14.84	−0.41 ± 9.79	+5.9
PCRTM_MRO4	+0.94 ± 23.19	−3.12 ± 14.36	−0.32 ± 9.81	+4.1
HT_CMO	+1.12 ± 23.41	−0.84 ± 14.99	+1.39 ± 9.65	+2.0
HT_CRO	+2.97 ± 23.08	−0.17 ± 14.68	+1.48 ± 9.58	+3.1
HT_CMRO	+1.17 ± 23.40	−0.78 ± 14.97	+1.40 ± 9.65	+2.0
HT_SMO	+0.92 ± 23.39	−1.08 ± 14.98	+1.15 ± 9.72	2.0
HT_SRO	+2.76 ± 23.06	−0.42 ± 14.68	+1.24 ± 9.65	3.2
HT_SMRO	+0.97 ± 23.38	−1.03 ± 14.96	+1.16 ± 9.72	2.0
RTTOV_MRO	−4.33 ± 22.32	−4.50 ± 14.49	−0.24 ± 9.77	0.2
RTTOV_CMSS	+2.71 ± 22.24	−2.35 ± 14.05	−0.06 ± 10.13	5.1
σ-IASI-As	+1.23 ± 22.35	+0.19 ± 14.45	+2.21 ± 9.34	1.0
CRTM_tcc	+2.60 ± 22.39	−2.76 ± 15.14	+0.73 ± 9.98	5.4
CRTM_mro	+1.95 ± 24.62	−5.60 ± 14.67	−1.68 ± 10.50	7.6
CRTM_2col	+2.94 ± 24.57	−5.24 ± 14.73	−1.69 ± 10.60	8.2

#### 4. Discussion of the Results

Under clear conditions at night, SARTA, PCRTM, and RTTOV have previously been shown to agree with each other and with AIRS within 0.05 K bias and 0.1 K stddev (Saunders et al., 2007). The current versions of SARTA, PCRTM, and RTTOV, including CRTM, σ-IASI, and HT-FRTC under clear conditions, all have shown the same level of agreement. Under cloudy conditions the agreement is not as close and the magnitudes of the differences are wavenumber dependent.

**Table 5**

*Histogram Correlation, Bias, and Standard Deviation at 2,616 cm<sup>−1</sup> for Day and Night Nonfrozen Ocean*

bt2616 (AIRS observed—calculated)	Day correlation	Day bias ± stddev (K) 1,437 cases	Night correlation	Night bias ± stddev (K) 1,377 cases
SARTA TwoSlab(C)	0.8744	+5.00 ± 14.79	0.9738	−3.06 ± 18.40
SARTA TwoSlab(P)	0.8779	+7.05 ± 15.57	0.9746	−0.37 ± 19.45
PCRTM_ERO	0.9855	+1.55 ± 15.90	0.9371	−0.29 ± 19.23
PCRTM_MRO	0.9846	+0.73 ± 15.84	0.9334	−1.88 ± 18.84
PCRTM_ERO2	0.9804	+2.52 ± 16.79	0.9563	+0.58 ± 20.56
PCRTM_MRO4	0.9766	+0.91 ± 16.22	0.9446	−1.25 ± 19.47
HT_CMO	0.6669	+15.04 ± 20.11	0.9075	−2.53 ± 20.49
HT_CRO	0.6492	+15.97 ± 19.76	0.9809	−1.43 ± 20.12
HT_CMRO	0.6653	+15.13 ± 20.10	0.9074	−2.46 ± 20.47
HT_SMO	0.9215	+3.69 ± 15.86	0.9791	−2.11 ± 20.59
HT_SRO	0.9628	+3.87 ± 15.83	0.9736	−0.83 ± 20.14
HT_SMRO	0.9245	+3.65 ± 15.88	0.9799	−2.02 ± 20.56
RTTOV_MRO	0.8948	+4.81 ± 15.86	0.9574	−6.48 ± 19.85
RTTOV_CMSS	0.8803	+8.07 ± 15.26	0.9605	−2.38 ± 19.02
σ-IASI_as	0.4809	+20.94 ± 18.94 <sup>(a)</sup>	0.8739	+5.37 ± 19.50
CRTM_tcc	0.3991	+20.55 ± 17.60	0.6623	+6.38 ± 20.52
CRTM_mro	0.6680	+13.90 ± 18.74	0.9604	−2.16 ± 19.58
CRTM_2col	0.6410	+15.33 ± 18.59	0.9486	−1.04 ± 19.63
Corr >0.9		7 of 18		16 of 18
Summary mean (stdev)		+2.4 (16)		−1.8 (20)

<sup>a</sup>Solar reflected component not implemented.

#### 4.1. The Longwave Region

We define the longwave region as portions of the spectrum with wavenumbers lower than  $1,700\text{ cm}^{-1}$ . In this region, the differences between AIRS and RTMs are relatively day/night independent (Figure 1) and range between  $\pm 4\text{ K}$ . The correlation between the histogram calculated from the AIRS observations and the histograms calculated for several of the RTMs at  $900\text{ cm}^{-1}$  (Table 2 and Figure 2) exceeds 0.97. The bias averaged over 17 of 18 RTMs at  $900\text{ cm}^{-1}$  for the day and night nonfrozen oceans was  $+0.3$  and  $+0.8\text{ K}$ , respectively (Table 2). However, Table 4 shows that the low bias for the nonfrozen oceans for some RTMs was due to the compensating effects of a bias for the tropical zone balanced by a bias of the opposite signs in the midlatitude and polar zones. A high correlation between the observed and calculated histograms and a zone-independent low bias are a measure of the skill of the RTM and the statistical fidelity of the ECMWF specification of the atmospheric state, including clouds. The bias between the clear column RTM calculations and AIRS observations is more than  $-25\text{ K}$  (Table 2). The typically  $20\text{ K}$  stddev of the difference between AIRS and the RTMs is essentially the same with and without clouds. This indicates that the high stddev of (AIRS-RTM) is dominated by the mismatch between the clouds observed by AIRS and the clouds specified by the ECMWF model.

RTTOV\_MRO is biased about  $4\text{-K}$  high relative to AIRS (Table 2). As shown in Table 3, where we compare the RTMs to reference RTMs, all RTMs are biased low relative to RTTOV\_MRO. RTTOV\_MRO used the OPAC cumulus cloud-type option. RTTOV\_Cloud fraction Maximum Single Stream (CMSS) used the RO overlap scheme and was optimized for middle to upper tropospheric sounding channels, not for window channels. RTTOV\_CMSS shows much less bias relative to AIRS than RTTOV\_MRO in the global analysis (Table 2) but shows a large bias of opposite signs for the zonal bias (Table 4). These observations suggest that a combination of cloud types (derived from the cloud, temperature, or water vapor profiles) may produce a closer match to observations than choosing one cloud type. Future work will examine the impact of cloud-type assumptions on the RTMs' match to observations.

The typical stddev of the RTMs relative to AIRS,  $20\text{ K}$ , decreases to a range of  $6$  to  $12\text{ K}$  when the RTMs are compared to one another (Table 3), excluding siblings within the same RTM group. Since the RTMs used the same cloud input profile, the decrease from  $20$  to  $12\text{ K}$  (or less) is dominated by the elimination of the collocation error. The stddevs of the differences are in this case related to differences in the way the ECMWF cloud description is converted to cloud microphysical parameters and then to the radiances calculated by the RTMs. When this conversion is identical, as in the case of CRTM\_mro and CRTM\_2col, the stddev of the difference was  $3\text{ K}$  and was due to the difference in the overlap assumption alone.

#### 4.2. The Shortwave Region

We define the shortwave region as portions of the spectrum with wavenumbers greater than  $2,000\text{ cm}^{-1}$ . By inspection of Figure 1 we already noted that the spectral patterns for the different RTMs are less consistent in the shortwave region than in the longwave region, even for the night data. However, at night three of the six RTMs (Figure 1) have less than  $2\text{-K}$  bias relative to AIRS and five of the six RTMs have histogram correlations better than 0.95 (Table 5). At night the histogram correlations at  $2,616\text{ cm}^{-1}$  are not inconsistent with those at  $900\text{ cm}^{-1}$ . During the day the results from only two of the six RTM teams reached histogram correlations better than 0.95, and the bias values relative to AIRS were much larger than those at night and the result at  $900\text{ cm}^{-1}$ . If cloud scattering parameters at  $2,616\text{ cm}^{-1}$  were too weak, it would have impacted the night calculations as well, but the night calculations (for three of the RTMs) agree reasonably well with AIRS. The degradation of the results during the day is probably related to the use of Chou scaling, which was not designed for shortwave calculations (Chou et al., 1999). This is clearly shown in the comparison of HT\_CRO (with the Chou approximation) and HT\_SRO (using full scattering) in Figure 3. The tail of the histogram of HT\_CRO at (stemp-bt2616) extends all the way to  $100\text{ K}$  for the coldest clouds, while the tail of the histogram of HT\_SRO stops at  $60\text{ K}$ . The PCRTM\_MRO also uses full scattering. SARTA and RTTOV used Chou scaling, while CRTM used the advanced doubling adding method (Liu & Weng, 2006). Full scattering calculations usually are assumed to be costly in terms of computation time, but this need not be the case. For example, PCRTM performs full scattering calculations with multiple streams and multiple scatterings performed offline to generate lookup tables. However, even by employing full scattering, the HT\_SRO histogram at  $2,616\text{ cm}^{-1}$  (Figure 3b) showed fewer clear or low cloud cases (stemp-bt2616  $< 0\text{ K}$ ) calculated by the RTMs than were observed by AIRS. This suggests that the reflectance from the Earth's surface has a stronger angular dependence than Lambertian scattering.



In the discussion of the histograms calculated from the RTMs at  $900\text{ cm}^{-1}$  we noted the differences between AIRS observations and the RTMs for  $40 < (\text{stemp-bt900}) < 70\text{ K}$  cases (Figure 2). This effect is much less pronounced at  $2,616\text{ cm}^{-1}$ , particularly at night (Figure 3a). We believe that in this region a significant portion of the scenes contains multiple cloud types. This may amplify any systematic bias that exists in the assumptions about cloud microphysics and their assumed spectral dependence. The interpretation of these differences in terms of cloud types is outside of the scope of this paper.

### 4.3. ECMWF Cloud Bias and RTM Cloud Bias

The bias in the RTMs relative to AIRS has two components:

1. The ECMWF cloud description is vulnerable to systematic errors.
2. The methodologies used by the RTMs to convert the cloud description into radiances are likely to contain assumptions which lead to systematic biases.

In order to quantify this bias, we assume that the results from the six RTM teams represent plausible and sufficiently independent radiometric realizations of the cloud effects. At  $900\text{ cm}^{-1}$  the RTMs show a bias in the range from  $+1.5$  to  $-3.4\text{ K}$  relative to one another (Table 3). Relative to AIRS the RTMs have a  $+0.3\text{ K}$  ( $+0.8\text{ K}$ ) mean bias for the day (night) nonfrozen oceans (Table 2). These results indicate that the radiative effect of a bias in the ECMWF clouds could be of the order of  $1\text{ K}$ .

The difference between the mean tropical and mean midlatitude bias (Table 4, last column) for each RTM could reveal a cloud-type dependence in the ECMWF clouds or in the RTM cloud algorithms. Several of the six RTM groups have a zonal bias lower than  $2\text{ K}$ . The low zonal bias seen in the results from these RTMs is consistent with the radiative effect of a zonal ECMWF cloud bias of less than  $2\text{ K}$ . The observation that several of the RTMs achieve a low zonal bias and a high histogram correlation relative to the observations indicates that the low global bias is not the result of compensatory much larger cloud-type-dependent biases.

We interpret the zonal bias seen in the three other RTM groups, which ranges from  $4$  to  $8\text{ K}$ , as a cloud-type dependence in those RTMs. The RTTOV\_CMSS has a  $5\text{-K}$  zonal bias, compared to  $0.2\text{ K}$  for RTTOV\_MRO (Table 4). On the other hand, RTTOV\_CMSS shows much less bias relative to AIRS than RTTOV\_MRO (Table 2). Both use a single (but different) cloud type. A combination of cloud types (derived from the cloud, temperature, or water vapor profiles) may produce a closer match to observations than choosing one cloud type. A future analysis of cloud-type effects on the RTMs could include data acquired in cloudy conditions from other instruments.

## 5. Summary

The objective of our paper was to evaluate the degree to which the radiative effects of clouds in NWC models agree with collocated hyperspectral observations. We selected AIRS observations and AIRS RTMs for our analysis. We selected data provided by the ECMWF (ECMWF, 2009) as representative for the definition of the atmospheric states with clouds. We used the bias and histogram correlations relative to AIRS observations for the  $2,616\text{-}$  and  $900\text{-cm}^{-1}$  atmospheric window channels as performance metrics. For some RTMs the histogram calculated at  $900\text{ cm}^{-1}$  has a correlation of better than  $0.95$  with the histogram derived from the AIRS observations, with a bias relative to AIRS of less than  $2\text{ K}$  for nonfrozen ocean day and night data. However, several of the six RTM groups showed between  $0\text{-}$  and  $2\text{-K}$  bias between the tropical zone and the midlatitude zone at  $900\text{ cm}^{-1}$ , while others had a bias between  $4$  and  $8\text{ K}$ . This observation and the high histogram correlation with AIRS show that the ECMWF cloud prescription may have a bias, but the radiative effect of the bias at  $900\text{ cm}^{-1}$  is most likely less than  $2\text{ K}$ , relatively insignificant compared to the bias introduced by some RTMs. The results for the  $2,616\text{-cm}^{-1}$  window channel are consistent with day and night results at  $900\text{ cm}^{-1}$  only when full scattering calculations were used. For these cases the correlation between the histogram deduced from the AIRS observations and the histograms calculated by the RTMs exceeds  $0.95$  and the bias at night is less than  $2\text{ K}$  relative to AIRS. During the day the AIRS observations at  $2616\text{ cm}^{-1}$  are  $2$  to  $4\text{ K}$  higher than the RTM calculations with full scattering. This suggests that the reflectance of the surface has a steeper angular dependence than Lambertian.

Our study created a testable data set, baseline results, and testing methodology to support continuing RTM development, with the goal of increasing the utilization of hyperspectral observations in the forecast. As

illustrated in Figure 1, there is no need (with the current state of the art RTMs) to make these calculations for all channels, since just one or two surface channels will provide valuable insights. However, the selection of a shortwave channel requires an RTM with full scattering. The choice of the RTM and how many channels to use comes down to computer resource requirements.

## Appendix A: Appendixes

### A1. Model Profiles (Contributed by Alan Geer)

Model profiles were taken from the ECMWF operational global weather forecasting system on 1 March 2009. The best available estimate of the atmospheric state was taken every 3 hr, being a mixture of analysis and very short range forecast. At the time, cycle 35r1 of the ECMWF system was operational and full documentation is available from ECMWF (2009). This describes cycle 33r1, but there were no major changes going to 35r1. The model fields used 91 levels. An additional level at 0.005 hPa was added using the U.S. Standard Atmosphere to avoid ambiguity when different RTMs were using the model fields. The forecast model uses T799 (roughly 25 km) spatial binning. Each AIRS position and observing time from 1 March 2009 was associated with the nearest forecast time and interpolated across the 35r1 grid points in time and space.

Analyses and forecasts are based on clouds and precipitation models using three main schemes: convection by a mass flux scheme (Bechtold et al., 2004; Tiedtke, 1989), large-scale cloud and precipitation, including the possibility of ice supersaturation (Tiedtke, 1993; Tompkins et al., 2007), and an eddy-mass flux turbulent diffusion scheme for the boundary layer, representing stratocumulus (Köhler et al., 2011). Together these contribute to producing the vertical profile of cloud water, cloud ice, and cloud fraction at every grid point. Where necessary to assume an overlap formulation for clouds in the radiation scheme, a generalized formulation was assumed, increasing from MRO to RO with increasing cloud layer separation (Barker, 2008).

The ECMWF analysis is a combination of short-range forecast and observational information, including satellite radiances, satellite-retrieved atmospheric motion vectors, near-surface wind vectors from scatterometers, Global Navigation Satellite System radio-occultation measurements, and conventional data sources including ground stations, ships, radiosondes, and aircraft. Of particular relevance to the current study is that AIRS and IASI radiances are assimilated but in clear-sky areas only (Collard & McNally, 2009). As a consequence, the cloud description in the ECMWF model does not contain AIRS cloud information. Further, clouds and precipitation are constrained in the analysis by the assimilation of cloud and precipitation-affected microwave imager radiances (Bauer et al., 2006).

### A2. Selection of the Test Data Set (Contributed by Evan Manning)

Each day AIRS produces 3 million spectra, each with 2,378 spectral channels. The locations of the spectra are biased toward the polar areas due to the high inclination of the Earth Observing System Aqua orbit. In order to test the relative performance of cloudy RTAs, we created a data set with emphasis on cloud variability. This data set was created using stratified sampling: the clouds are roughly characterized by the difference between the surface temperature (stemp), provided by ECMWF, and the brightness temperatures measured in five sounding regions from AIRS, including the brightness temperatures at  $1,231\text{ cm}^{-1}$  (bt1231). We traversed the spectra in time order and assigned to each spectrum a tag which combined the following elements:

1. Day versus night (the divide was solar zenith angle = 90; two bins).
2. Land/sea + latitude band. The  $30^\circ$  bins. Nonpolar bins were divided into land and sea. Sea was defined as any AIRS footprint containing less than 1% land (10 bins).
3. bt1231 in 10-K increments between 170 and 360 K (19 bins).
4. stemp-bt1231 in 10-K increments from  $-40$  to  $+210$  K (26 bins).
5. We defined five broad spectral bands at [650, 800], [800, 1200], [1200, 1700], [1700, 2400], and [2400, 2700]  $\text{cm}^{-1}$ . For each band we used the mean brightness temperature in the band minus bt1231,  $\text{bt\_band-bt1231}$ , to define 20 bins in 10-K increments from  $-110$  to  $+110$  K (20 bins per band).

This allows for up to  $2 \times 10 \times 19 \times 26 \times 20^5 = \sim 30$  billion bins, but most bins were empty. Each spectrum's tag was compared to the tags of the spectra previously collected. If the tag did not match any, then the new spectrum was added to the data set. This procedure created 7,377 uniquely tagged spectra. The latitude,

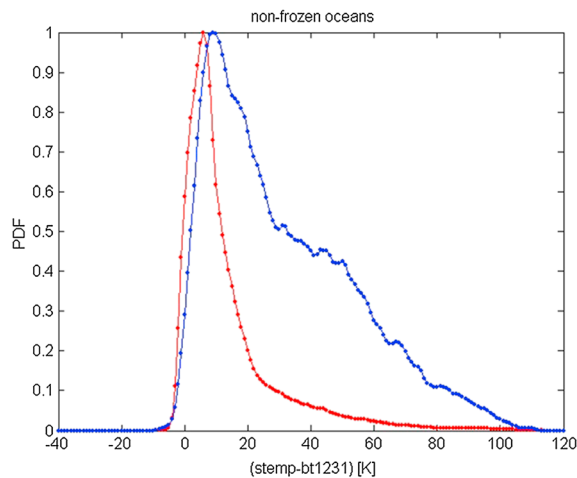


**Figure A1.** The red trace shows the distribution of the cloud effect (stemp-bt1231) for an area-representative random sample of the nonfrozen oceans. The blue trace is the distribution of the stratified sample.

longitude, solar zenith, and solar azimuth angles and the ECMWF definition of the state of the atmosphere associated with this set and the associated AIRS spectral radiances were posted on the anonymous FTP site at “ftp://thunder.jpl.nasa.gov/hha/Cloudy\_RTAtm.state”. The rta7377readme.20160518.txt explains the details.

The distribution of the 7,377 test cases does not match the distribution of clouds in a global grid, but the set spans the natural variability of spectra, which is dominated by clouds. The emphasis on clouds is illustrated in Figure A1. The red trace in Figure A1 is the distribution of the cloud effect (stemp-bt1231) for a global area representative random sample of the nonfrozen oceans. A large fraction of the ocean is covered by relatively low or broken clouds. The peak of the random sampled distribution is at 5 K. Only 7% of the nonfrozen oceans are associated (stemp-bt1231) > 50 K, (roughly corresponding to brightness temperatures colder than 250 K). The blue trace in Figure A1 is the distribution of the cloud effect in the test set. The peak of the distribution is at 8 K, and 30% of the test data are associated with (stemp-bt1231) > 50 K.

### A3. RTM Model Summaries

#### A3.1. Community RTM (Contributed by Moradi and Wilson)

The Community RTM, CRTM, (Liu et al., 2008), is a fast RTM developed by the Joint Center for Satellite Data Assimilation that is widely used in the United States (including at the National Aeronautics and Space Administration Global Modeling and Assimilation Office) to assimilate satellite radiances. The current version is 2.2.3. CRTM is capable of simulating microwave and infrared radiances using atmospheric profiles of pressure, temperature, humidity, and other species such as ozone. CRTM also includes capabilities to simulate satellite cloudy radiances. The ice cloud single scattering properties are based on Baum et al. (2011). All spectra were calculated with CRTM 2.2.3. However, within this version CRTM gives the user wide flexibility for the cloud overlap assumption and the cloud composition. Six cloud types can be defined at the same time: water, ice, rain, snow, graupel, and hail. The calculations presented in this paper used only water and ice clouds based on cloud liquid and ice water content profiles.

CRTM requires pressure values at levels, as well as layer averaged, and the layer averages of temperature, water vapor, and other absorbers as input to perform clear-sky calculations. The top pressure level is fixed at 0.005 hPa. For the calculation of cloudy radiances CRTM requires cloud liquid water content in gram per square meter and the effective radii of water and ice particles.

The same version of CRTM was used but with different assumptions. The results identified as CRTM\_tcc uses equation (1) with the MO assumption and tcc, the total cloud fraction specified by ECMWF. The effective radius of the particles was calculated using equation (3) in Ou et al. (1995) for ice clouds and equation (2) in Bower et al. (1994) for water clouds. The CRTM\_2col and the CRTM\_mro calculations used the 2col and MRO assumption, respectively, with the identical cloud microphysics. The parameterization for ice particle effective radius used a fourth-order empirical polynomial given by Ou et al. (1995), same as CRTM\_tcc. The effective water particle radius was logarithmically interpolated from 10  $\mu\text{m}$  at the surface to 45  $\mu\text{m}$  at the top of atmosphere, consistent with the ECMWF documentation. Following equation (1), CRTM\_2col uses the maximum cloud fraction specified by each ECMWF cloud coverage profile to calculate CF. This value is close to but not exactly the same as tcc.

The CRTM results were received on 6 September 2016, revised 9 March 2017.

#### A3.2. Principal Component-Based RTM (Contributed by Xiuhong Chen, Xianglei Huang, Xu Liu, Qiguang Yang, and Wan Wu)

The PCRTM is a fast and accurate forward model for hyperspectral instruments with thousands of spectral channels. It uses principal components to compress spectral information and reduces computational time by performing radiative transfer calculations at just a few hundred monochromatic frequencies (Liu et al., 2006, 2016). The molecular absorption coefficients of gases are based on a lookup table calculated off-line using a line-by-line RTM based on HITRAN2008. Both ice and water clouds were parameterized into

transmittance and reflectance matrices for the isotropic thermal scattering. The ice cloud matrices were obtained using single scattering properties from Baum et al. (2011) and a 32-stream Discrete Ordinates Radiative Transfer (Stamnes et al., 1988). The water clouds were obtained the same way by using the refractive indices from Segelstein (1981). The anisotropic solar scattering is modeled according to Liu et al. (2016) and Yang et al. (2014). Transmittance and reflectance lookup tables were obtained under various conditions for parameters such as cloud optical depth, cloud effective size, wavelength, and solar and satellite zenith angles and azimuth angles (Yang et al., 2014). The non-Local Thermodynamic Equilibrium (LTE) effect was calculated according to the parameterization described by DeSouza-Machado et al. (2007).

When generating input parameters for the PCRTM from the ECMWF fields, ice cloud optical depths were calculated from ice water content as in Ebert and Curry (1992). Warm cloud optical depth based on cloud liquid water content follows Fouquart (1987). The effect of different cloud overlapping assumptions on the simulated radiance has been discussed in Chen et al. (2013). The PCRTM\_MRO and PCRTM\_ERO entries in Tables 2–4 represent the results obtained with a MRO assumption and an ERO assumption, respectively. The cloud fraction and cloud profiles are used to generate 50 subcolumns (Chen et al., 2013) for both overlapping assumptions. The PCRTM\_ERO2 and PCRTM\_MRO4 represent the simulation results using less subcolumns, namely, two subcolumns for the ERO and four subcolumns for the MRO, respectively.

The PCRTM model has been used to perform cloud and atmospheric temperature and water vapor vertical profile retrievals from hyperspectral instruments such as IASI, CrIS, and AIRS (Liu et al., 2009, 2006, 2017; Wu et al., 2017). Two validations of the PCRTM under cloudy conditions were given by Chen et al. (2013). One validation case used NOAA/GFDL data with the RO assumption, and the other one used ECMWF with MRO assumption. Validations showed satisfactory consistency between the calculated OLR and the counterparts from the GCM/analysis.

The PCRTM spectra were received 24 February 2017, revised with full scattering 14 July 2017.

### **A3.3. SARTA (Contributed by Sergio DeSouza-Machado and L. Strow)**

SARTA RTM uses a four-column RO cloud overlap assumption. The clear column calculations use SARTA V6.0 (Strow et al., 2006). The absorption coefficients of gases are from line-by-line calculations based on HITRAN2008. The ECMWF clouds are converted into two thick slabs. Typically, this is an ice cloud between  $z_{i\_top}$  and  $z_{i\_bottom}$  and a water cloud between  $z_{w\_top}$  and  $z_{w\_bottom}$ . The Mie scattering parameters for water clouds use a modified gamma droplet size distribution of effective variance 0.1 (dimensionless) and effective radius (typically) of 20  $\mu\text{m}$ . The cirrus cloud scattering parameters are based on Baum et al. (2011), and the ice effective particle size is estimated from a temperature-based parametrization by Ou et al. (1995, 2013), where the ECMWF temperature profile is used to associate the ice cloud slab top pressure with a cloud top temperature. The effective absorption due to each slab is then calculated using PCLSAM (Chou et al., 1999) scattering code and used in the SARTA TwoSlab RTM (DeSouza-Machado et al., 2018). Each pixel is then divided into four columns.

Case 1. A clear column from the surface to the Top Of the Atmosphere (TOA).

Case 2. A clear column between the surface and  $z_{w\_bottom}$ . Between  $z_{w\_bottom}$  and  $z_{w\_top}$  the pre-calculated water cloud absorption is added.

Case 3. A clear column between the surface and  $z_{i\_bottom}$ . Between  $z_{i\_bottom}$  and  $z_{i\_top}$  the pre-calculated ice cloud absorption is added.

Case 4. The transmittance calculated from case 2 up to the  $z_{i\_bottom}$  is continued with the transmittance from there to TOA using the transmittance calculated from case 3.

A cloud fraction for each case is then chosen such that all of the ice cloud and a random portion of the water cloud is seen from TOA, such that the ECMWF-specified  $tcc$  is satisfied. Details are summarized in Machado and Strow (2016) and in DeSouza-Machado et al. (2018). The difference between SARTA\_TwoSlab(C) and SARTA\_TwoSlab(P) is due to the difference in the way the boundaries of the thick slabs are calculated. The small differences between the results from the two SARTA versions show that the results are not very sensitive to these details.

The SARTA results were received 8 November 2016, revised to be consistent with DeSouza-Machado et al. (2018) 27 February 2017.

### **A3.4. Radiative Transfer for TOVS (Contributed by J. Vidot and M. Matricardi)**

The fast RTM RTTOV (Saunders et al., 1999) is widely used by a number of NWCs to assimilate infrared radiance observations. In this study, we used RTTOV Version 12. The predictors of the fast atmospheric

transmittances were calculated with the line-by-line model LBLRTM 12.2 (Alvarado et al., 2013; Clough et al., 2005) that uses the AER3.2 spectroscopic database (mostly based on HITRAN 2008 but with many improvements regarding line mixing and absorption line parameters) and MTCKD 2.5.2 (Mlawer et al., 2012). The scattering by clouds is modeled using the Chou-scaling approximation (Chou et al., 1999). The liquid and ice cloud optical properties are parameterized following the work of Matricardi (2005) and Vidot et al. (2015), respectively. Within the RTTOV version the user has the option to select a limited number of cloud type and the cloud overlap assumptions. RTTOV\_mro used the OPAC cumulus cloud type and the MRO assumption (Matricardi, 2005). Additionally, a much faster, experimental version of the cloud overlap method has been tested in RTTOV. This method is named CMSS. It simulates cloudy infrared radiances using equation (1) with CF set to the maximum cloud fraction in the layers above a certain pressure level (here fixed to 750 hPa). This method is optimized for middle- and upper-tropospheric sounding channels.

The RTTOV results were received 9 December 2016.

### A3.5. Havemann-Taylor Fast Radiative Transfer Code (Contributed by Havemann)

For the AIRS radiance simulations presented in this paper, the HT-FRTC (Havemann, 2006) has been specifically trained for the infrared part of the electromagnetic spectrum. The HT-FRTC does only monochromatic radiative transfer calculations. The gaseous absorption of all the trace gases included in HITRAN 2008 is included in the form of lookup tables. During the code training phase monochromatic calculations are performed at a very high spectral resolution ( $10^{-3} \text{ cm}^{-1}$ ) for a diverse set of 1,000 atmospheric profiles and surface conditions. The training run included vertical profiles of liquid and ice cloud. The results of the radiance calculations for the training profiles at the very high spectral resolution were then used to calculate the principal components which are the eigenvectors of the covariance matrix containing the radiance spectra. The HT-FRTC works slightly different to other codes like PCRTM in that the principal components are not derived for the spectra of any particular instrument but rather at the full very high spectral resolution. This means that the spectra for any number of instruments can be calculated in a single fast code run. It requires just an offline convolution of the highly resolved principal components with the instrument response functions. For the simulations in this paper only the first 100 principal components which contain most of the variance were used. The weights of the principal components are predicted from a small number of radiance calculations at about 100 monochromatic frequencies. The optimal set of frequencies for prediction is selected by a k-means clustering algorithm which operates on all frequencies (2.5 million). A linear regression is carried out on the results on the training profiles (the dependent profiles). This regression then allows the prediction of the principal component weights for any independent profiles by calculating the radiances only at the 100 selected monochromatic frequencies.

For the simulations presented in this paper an effective radius of  $10 \mu\text{m}$  was used throughout for cloud liquid droplets. The cirrus optical properties that were used in the simulations are due to Baran (Baran et al., 2014). Baran has developed an ensemble model of cirrus particles of different shapes and sizes. The optical properties are parametrized solely in terms of cirrus cloud temperature and cirrus cloud ice water content. The same parametrization is applied to all types of cirrus. The HT-FRTC allows two different treatments of scattering. Scattering can be treated approximately as a modification to the extinction by using the Chou scaling approximation (Chou et al., 1999) or the scattering phase function that can be fully accounted for (Martinet et al., 2013). In this case a monochromatic version of the Edwards-Slingo spherical harmonics radiation code is called which has been incorporated into the HT-FRTC (Edwards & Slingo, 1996; Thelen & Edwards, 2013). Calculations with Chou scaling are indicated by "C" and full scattering calculations by "S".

The HT-FRTC has been run for three different cloud overlap assumptions (MRO, MO, and RO). In all cases five cloud columns were used. The columns were constructed from the horizontal cloud fraction provided for each atmospheric level, which prescribed how many of the cloud columns would be clear and how many fully overcast at each level. The different overlap assumptions then determine how the cloudy layers are stacked in the vertical. In the case of MO, all the cloudy layers are concentrated in the same columns as much as possible, in the case of RO the cloudy layers are distributed randomly across the columns, and in the case of MRO the cloudy columns are maximally overlapped in adjacent vertical layers which are both cloudy but randomly distributed if there happens to be a cloud-free layer in between. One HT-FRTC fast code run is done per cloud column. In the tables the type of scattering treatment and the kind of overlap is indicated. As an example, SMRO indicates full scattering calculations applied to the five individual cloud columns that were generated using the MRO assumption.



The HTFRTC results were received with Chou scaling 19 January 2017, revised with full scattering 17 April 2017.

### A3.6. The $\sigma$ -IASI-as (Contributed by Liuzzi, Masiello, and Serio)

The  $\sigma$ -IASI-as RTM is an advanced version of the  $\sigma$ -IASI model (Amato et al., 2002) with respect to cloud and aerosol treatment (Liuzzi et al., 2017). The model computes the Earth/atmosphere-emitted radiance in the spectral range 100–3,000  $\text{cm}^{-1}$ . In its current version, the model can generate radiances in both upwelling and downwelling modes. Although initially developed for IASI,  $\sigma$ -IASI-as is presently a generic RTM, which is well suited for nadir viewing satellite, airplane (Grieco et al., 2007), and ground-based (Bhavar et al., 2008) infrared sensors with a sampling rate in the range 0.1–2  $\text{cm}^{-1}$ .

The  $\sigma$ -IASI-as RTM calculation of gas optical depths is based on a pseudomonochromatic scheme, in which transmittances are calculated on an equally spaced wavenumber grid by means of a lookup table. For each atmospheric layer, atmospheric species, and wavenumbers, optical depths are precomputed and stored. Then, they are rescaled with air pressure and temperature. The dependence on temperature is parameterized by a second-order polynomial. This allows optical depths to be generated at any wavenumber using the version 12.2 of LBLRTM (Clough et al., 2005), equipped with the spectral library AER v\_3.2 (essentially based on HITRAN 2012 spectral database—with the continuum model MT-CKD v\_2.5.2; Mlawer et al., 2012).

The  $\sigma$ -IASI-as RTM simulates the impact of the presence of clouds and aerosols with a physically based method that computes their extinction as a function of the effective ice or liquid water particle or droplet radii and concentrations (Liuzzi et al., 2017). The model exploits an ab-initio approach embodying Mie routines which are called iteratively within the calculation of single-layer transmittances. The results of Mie calculations are manipulated according to the scheme described in Chou et al. (1999) for calculating effective aerosol and cloud optical depths taking into account the multiple scattering effects through the so-called scaling approximation. With the scaling approximation, radiative transfer equations for a cloudy/aerosols atmosphere are identical to those for a clear atmosphere, and the difficulties in applying a multiple-scattering algorithm to a partly cloudy atmosphere (assuming homogeneous clouds) are avoided. The RTM used for the calculation of the  $\sigma$ -IASI spectra was identified as version 2017.as.lr. The calculations used the MO assumption and tcc specified by ECMWF.

The  $\sigma$ -IASI results were received on 29 November 2016, revised 17 March 2017.

### Acknowledgments

The work described in this paper was carried out at the Jet Propulsion Laboratory, California Institute of Technology, under a contract with the National Aeronautics and Space Administration. Work at JPL and UMBC was funded by NASA ROSES, with the longtime support of Ramesh Kakar of NASA Headquarters. Steve Broberg helped with technical editing. The work at LARC was supported by NASA NAST-1 and CLARREO projects. The work at NASA/GMAO was funded under NASA grant NNX17AE79A Goddard Space Flight Center Cooperative Agreement. The work at the University of Michigan was supported by NASA grant NNX15AC25G. The work at Meteo France was supported by the EUMETSAT NWP-SAF program. The work at the UK Met Office was supported as part of the science program theme “Improved use of Satellite Data”. The 7,377 atmospheric states and associated AIRS spectra used for this paper can be found at [ftp://thunder.jpl.nasa.gov/hha/Cloudy\\_RTA](ftp://thunder.jpl.nasa.gov/hha/Cloudy_RTA). The file `readme.20160518.txt` defines various parameters. The file `AIRS_SRF_m140f.mat` defines the AIRS SRF for each of the 2,378 channels in a MATLAB Version 7.0 format.

### References

- Alvarado, M. J., Payne, V. H., Mlawer, E. J., Uymin, G., Shephard, M. W., Cady-Pereira, K. E., et al. (2013). Performance of the line-by-line radiative transfer model (LBLRTM) for temperature, water vapor, and trace gas retrievals: Recent updates evaluated with IASI case studies. *Atmospheric Chemistry and Physics*, 13(14), 6687–6711. <https://doi.org/10.5194/acp-13-6687-2013>
- Amato, U., Masiello, G., Serio, C., & Viggiano, M. (2002). The sigma-IASI code for the calculation of infrared atmospheric radiance and its derivatives. *Environmental Modelling and Software*, 17, 651–667. [https://doi.org/10.1016/S1364-8152\(02\)00027-0](https://doi.org/10.1016/S1364-8152(02)00027-0)
- Aumann, H. H., Chahine, M. T., Gautier, C., Goldberg, M., Kalnay, E., McMillin, L., et al. (2003). AIRS/AMSU/HSB on the Aqua mission: Design, science objectives, data products and processing systems. *IEEE Transactions on Geoscience and Remote Sensing*, 41(2), 253–264.
- Baran, A. J., Cotton, R., Havemann, S., Furtado, K., Marengo, F., Smith, A., et al. (2014). A self-consistent scattering model for cirrus. II. The high and low frequencies. *Quarterly Journal of the Royal Meteorological Society*, 140(680), 1039–1057. <https://doi.org/10.1002/qj.2193>
- Barker, H. W. (2008). Representing cloud overlap with an effective decorrelation length: An assessment using CloudSat and CALIPSO data. *Journal of Geophysical Research*, 113, D24205. <https://doi.org/10.1029/2008JD010391>
- Bauer, P., Lopez, P., Salmond, D., Benedetti, A., Saarinen, S., & Bonazzola, M. (2006). Implementation of 1D+ 4D-Var assimilation of precipitation-affected microwave radiances at ECMWF. II: 4D-Var. *Quarterly Journal of the Royal Meteorological Society*, 132(620), 2307–2332.
- Baum, B., Yang, P., Heymsfield, A., Schmitt, C., Xie, Y., Bansemir, A., et al. (2011). Improvements to shortwave bulk scattering and absorption models for the remote sensing of ice clouds. *Journal of Applied Meteorology and Climatology*, 50(5), 1037–1056. <https://doi.org/10.1175/2010JAMC2608.1>
- Bechtold, P., Chaboureaud, J. P., Beljaars, A., Betts, A. K., Köhler, M., Miller, M., & Redelsperger, J. L. (2004). The simulation of the diurnal cycle of convective precipitation over land in a global model. *Quarterly Journal of the Royal Meteorological Society*, 130(604), 3119–3137.
- Bennartz, R., & Greenwald, T. (2011). Current problems in scattering radiative transfer modelling for data assimilation. *Quarterly Journal of the Royal Meteorological Society*, 137(661), 1952–1962. <https://doi.org/10.1002/qj.953>
- Bhavar, R., Bianchini, G., Bozzo, A., Cacciani, M., Calvello, M. R., Carlotti, M., et al. (2008). Spectrally resolved observations of atmospheric emitted radiance in the H<sub>2</sub>O rotation band. *Geophysical Research Letters*, 35, L04812. <https://doi.org/10.1029/2007GL032207>
- Blumstein, D., Chalon, G., Carlier, T., Buil, C., Hebert, P., Maciaszek, T., et al. (2008). IASI instrument: Technical overview and measured performances. In M. Strojnik (Ed.), *Infrared spaceborne remote sensing XII, Proc SPIE* (Vol. 5543, pp. 196–207).
- Bower, K. N., Choullarton, T. W., Latham, J., Nelson, J., Baker, M. B., & Jensen, J. (1994). A parameterization of warm clouds for use in atmospheric general circulation models. *Journal of the Atmospheric Sciences*, 51(19), 2722–2732. [https://doi.org/10.1175/1520-0469\(1994\)051<2722:APOWCF>2.0.CO;2](https://doi.org/10.1175/1520-0469(1994)051<2722:APOWCF>2.0.CO;2)

- Chen, X., Huang, X., & Liu, X. (2013). Non-negligible effects of cloud vertical overlapping assumptions on longwave spectral fingerprinting studies. *Journal of Geophysical Research: Atmospheres*, *118*, 7309–7320. <https://doi.org/10.1002/jgrd.50562>
- Chou, M.-D., Lee, K.-T., Tsay, S.-C., & Fu, Q. (1999). Parameterization for cloud longwave scattering for use in atmospheric models. *Journal of Climate*, *12*(1), 159–169. <https://doi.org/10.1175/1520-0442-12.1.159>
- Clough, S. A., Shephard, M. W., Mlawer, E. J., Delamere, J. S., Iacono, M. J., Cady-Pereira, K., et al. (2005). Atmospheric radiative transfer modeling: A summary of the AER codes, short communication. *Journal of Quantitative Spectroscopy & Radiative Transfer*, *91*(2), 233–244. <https://doi.org/10.1016/j.jqsrt.2004.05.058>
- Collard, A. D., & McNally, A. P. (2009). The assimilation of infrared atmospheric sounding interferometer radiances at ECMWF. *Quarterly Journal of the Royal Meteorological Society*, *135*(641), 1044–1058. <https://doi.org/10.1002/qj.410>
- DeSouza-Machado, S., Strow, L. L., Hannon, S. E., Motteler, H. E., López-Puertas, M., Funke, B., & Edwards, D. P. (2007). Fast forward radiative transfer modeling of 4.3  $\mu\text{m}$  nonlocal 965 thermodynamic equilibrium effects for infrared temperature sounders. *Geophysical Research Letters*, *34*, L01802. <https://doi.org/10.1029/2006GL026684>
- DeSouza-Machado, S., Strow, L. L., Tangborn, A., Huang, X., Chen, X., Liu, X., et al. (2018). Single-footprint retrievals for AIRS using a fast TwoSlab cloud-representation model and the SARTA all-sky infrared radiative transfer algorithm. *Atmospheric Measurement Techniques*, *11*(1), 529–550. <https://doi.org/10.5194/amt-11-529-2018>
- Ebert, E. E., & Curry, J. A. (1992). A parameterization of ice cloud optical properties for climate models. *Journal of Geophysical Research*, *97*(D4), 3831–3836. <https://doi.org/10.1029/91JD02472>
- European Center for Medium-Range Weather Forecasting (ECMWF) (2009). "IFS documentation Cy33r1". Retrieved from <http://www.ecmwf.int/en/forecasts/documentation-and-support>
- Edwards, J. M., & Slingo, A. (1996). Studies with a flexible new radiation code. I. Choosing a configuration for a large scale model. *Quarterly Journal of the Royal Meteorological Society*, *122*(531), 689–719. <https://doi.org/10.1002/qj.49712253107>
- Errico, R. M., Bauer, P., & Mahfouf, J. F. (2007). Issues regarding the assimilation of cloud and precipitation data. *Journal of the Atmospheric Sciences*, *64*(11), 3785–3798. <https://doi.org/10.1175/2006jas2044.1>
- Fouquart, Y. (1987). Radiative transfer in climate models. In M. E. Schlesinger (Ed.), *Physically based modelling and simulation of climate and climate changes* (pp. 223–284). Norwell, Mass: Kluwer Acad.
- Geer, A. J., Baordo, F., Bormann, N., Chambon, P., English, S. J., Kazumori, M., et al. (2017). The growing impact of satellite observations sensitive to humidity, cloud and precipitation. *Quarterly Journal of the Royal Meteorological Society*, *143*(709), 3189–3206. <https://doi.org/10.1002/qj.3172>
- Glumb, R. J., Williams, F. L., Funk, N., Chateaufort, F., Roney, A., & Allard, R. (2003). Cross-track infrared sounder (CrIS) development status. *Proceedings of SPIE*, *5152*.
- Grieco, G., Masiello, M., Matricardi, C., Serio, D. S., & Cuomo, V. (2007). Demonstration and validation of the IASI inversion scheme with NAST-I data. *Quarterly Journal of the Royal Meteorological Society*, *133*(53), 217–232. <https://doi.org/10.1002/qj.162>
- Guidard, V., Fourrié, N., Brousseau, P., & Rabier, F. (2011). Impact of IASI assimilation at global and convective scales and challenges for the assimilation of cloudy scenes. *Quarterly Journal of the Royal Meteorological Society*, *137*(661), 1975–1987. <https://doi.org/10.1002/qj.928>
- Havemann, S. (2006). The development of a fast radiative transfer model based on an empirical orthogonal functions (EOF) technique. *SPIE*, *6405*, 348–358.
- Hilton, F., Armante, R., August, T., Barnett, C., Bouchard, A., Camy-Peyret, C., et al. (2012). Hyperspectral Earth observation from IASI, five years of accomplishments. *Bulletin of the American Meteorological Society*, *93*(3), 347–370. <https://doi.org/10.1175/BAMS-D-11-00027.1>
- Hogan, R. J., & Illingworth, A. J. (2000). Deriving cloud overlap statistics from radar. *Quarterly Journal of the Royal Meteorological Society*, *126*(569), 2903–2909. <https://doi.org/10.1002/qj.49712656914>
- Kazumori, M., Geer, A. J., & English, S. J. (2016). Effects of all-sky assimilation of GCOM-W/AMSR2 radiances in the ECMWF numerical weather prediction system. *Quarterly Journal of the Royal Meteorological Society*, *142*(695), 721–737. <https://doi.org/10.1002/qj.2669>
- Köhler, M., Ahlgrimm, M., & Beljaars, A. (2011). Unified treatment of dry convective and stratocumulus-topped boundary layers in the ECMWF model. *Quarterly Journal of the Royal Meteorological Society*, *137*(654), 43–57. <https://doi.org/10.1002/qj.713>
- Lavanant, L., Fourrié, N., Gambacorta, A., Grieco, G., Heilliette, S., Hilton, F. I., et al. (2011). Comparison of cloud products within IASI footprints for the assimilation of cloudy radiances. *Quarterly Journal of the Royal Meteorological Society*, *137*(661), 1988–2003. <https://doi.org/10.1002/qj.917>
- Liu, Q., Liu, X., Liu, Y., Nalli, N. R., & Tan, C. (2017). *Fast radiative transfer algorithms for real-time sounder applications, Chapter in book reference module in Earth systems and environmental sciences*. New York: Elsevier Publishing. <https://doi.org/10.1016/B978-0-12-409548-9.10391-4>
- Liu, Q., & Weng, F. (2006). Advanced doubling-Adding method for radiative transfer in planetary atmospheres. *Journal of the Atmospheric Sciences*, *63*(12), 3459–3465. <https://doi.org/10.1175/JAS3808.1>
- Liu, Q., Weng, F., Han, Y., & VanDelst, P. (2008). Community Radiative Transfer Model for Scattering Transfer and Applications. Geoscience and Remote Sensing Symposium, IGARSS 2008. Retrieved from <https://ieeexplore.ieee.org/document/4779942?reload=true>
- Liu, X., Smith, W. L., Zhou, D. K., & Larar, A. (2006). Principal component-based radiative transfer model for hyperspectral sensors: Theoretical concept. *Applied Optics*, *45*(1), 201–209. <https://doi.org/10.1364/AO.45.000201>
- Liu, X., Yang, Q., Li, H., Jin, Z., Wu, W., Kizer, S., et al. (2016). Development of a fast and accurate PCRTM radiative transfer model in the solar spectral region. *Applied Optics*, *55*(29), 8236–8247. <https://doi.org/10.1364/AO.55.008236>
- Liu, X., Zhou, D. K., Larar, A. M., Smith, W. L., Schluessel, P., Newman, S. M., et al. (2009). Retrieval of atmospheric profiles and cloud properties from IASI spectra using super-channels. *Atmospheric Chemistry and Physics*, *9*(23), 9121–9142. <https://doi.org/10.5194/acp-9-9121-2009>
- Liuzzi, G., Masiello, G., Serio, C., Meloni, D., Di Biagio, C., & Formenti, P. (2017). Consistency of dimensional distributions and refractive indices of desert dust measured over Lampedusa with IASI radiances. *Atmospheric Measurement Techniques*, *10*(2), 599–615. <https://doi.org/10.5194/amt-10-599-2017>
- Machado, S. D., & Strow, L. L. (2016). "An accurate two-slab cloud-representation model for hyperspectral infrared radiative transfer codes", AGU2016 (A11P-01).
- Martinet, P., Fourrié, N., Guidard, V., Rabier, F., Montmerle, T., & Brunel, P. (2013). Towards the use of microphysical variables for the assimilation of cloud-affected infrared radiances. *Quarterly Journal of the Royal Meteorological Society*, *139*(674), 1402–1416. <https://doi.org/10.1002/qj.2046>
- Matricardi, M. (2005). The inclusion of aerosols and clouds in RT-IASI, the ECMWF fast radiative transfer model for the IASI, ECMWF Tech. Memo. 474 (53 pp.). Reading, UK: ECMWF
- McNally, A. P. (2009). The direct assimilation of cloud-affected satellite infrared radiances in the ECMWF 4D-Var. *Quarterly Journal of the Royal Meteorological Society*, *135*(642), 1214–1229. <https://doi.org/10.1002/qj.426>

- McNally, A. P., & Watts, P. D. (2003). A cloud detection algorithm for high-spectral-resolution infrared sounders. *Quarterly Journal of the Royal Meteorological Society*, *129*(595), 3411–3423. <https://doi.org/10.1256/qj.02.208>
- Mlawer, E. J., Payne, V. H., Moncet, J.-L., Delamere, J. S., Alvarado, M. J., & Tobin, D. D. (2012). Development and recent evaluation of the MT\_CKD model of continuum absorption. *Philosophical Transactions of the Royal Society A*, *370*, 1–37. <https://doi.org/10.1098/rsta.2011.0295>
- Okamoto, K., McNally, A. P., & Bell, W. (2014). Progress towards the assimilation of all-sky infrared radiances: An evaluation of cloud effects. *Quarterly Journal of the Royal Meteorological Society*, *140*(682), 1603–1614. <https://doi.org/10.1002/qj.2242>
- Ou, S. C., Liou, K. N., Takano, Y. Y., Rao, N. X., Fu, Q. Q., Heymsfield, A. J., et al. (1995). Remote sounding of cirrus cloud optical depths and ice crystal sizes from AVHRR data: Verification using FIRE II IFO measurements. *Journal of the Atmospheric Sciences*, *52*, 4143–4158. <https://doi.org/10.1175/1520-0469>
- Ou, S. S. C., Kahn, B. H., & Liou, K.-N. (2013). Retrieval of cirrus cloud properties from the atmospheric infrared sounder: The k-coefficient approach combined with SARTA plus delta-four stream approximation. *IEEE Transactions on Geoscience and Remote Sensing*, *51*, 1010–1024.
- Pavelin, E. G., English, S. J., & Eyre, J. R. (2008). The assimilation of cloud-affected infrared satellite radiances for numerical weather prediction. *Quarterly Journal of the Royal Meteorological Society*, *134*(632), 737–749. <https://doi.org/10.1002/qj.243>
- Saunders, R., Matricardi, M., & Brunel, P. (1999). An improved fast radiative transfer model for assimilation of satellite radiance observations. *Quarterly Journal of the Royal Meteorological Society*, *125*(556), 1407–1425. <https://doi.org/10.1002/qj.1999.49712555615>
- Saunders, R., Ray, P., Brunel, P., von Engeln, A., Bormann, N., Strow, L., et al. (2007). A comparison of radiative transfer models for simulating Atmospheric Infrared Sounder (AIRS) radiances. *Journal of Geophysical Research*, *112*, D01S90. <https://doi.org/10.1029/2006JD007088>
- Segelstein, D. (1981). The complex refractive index of water, (Master's thesis). University of Missouri, Kansas City.
- Stamnes, K., Tsay, S. C., Wiscombe, W., & Jayaweera, K. (1988). Numerically stable algorithm for discrete-ordinate-method radiative transfer in multiple scattering and emitting layered media. *Applied Optics*, *27*, 2502–2509.
- Strow, L. L., Hannon, S. E., DeSouze-Machado, S., Mottler, H. E., & Tobin, D. C. (2006). Validation of the atmospheric infrared sounder radiative transfer algorithm. *Journal of Geophysical Research*, *111*, D09S06. <https://doi.org/10.1029/2005JD006146>
- Thelen, C., & Edwards, J. M. (2013). Short-wave radiance comparisons between SEVERI and the Unified Model. *Quarterly Journal of the Royal Meteorological Society*, *139*(675), 1665–1679. <https://doi.org/10.1002/qj.2034>
- Tiedtke, M. (1989). A comprehensive mass flux scheme for cumulus parameterization in large-scale models. *Monthly Weather Review*, *117*(8), 1779–1800. [https://doi.org/10.1175/1520-0493\(1989\)117<1779:ACMFSF>2.0.CO;2](https://doi.org/10.1175/1520-0493(1989)117<1779:ACMFSF>2.0.CO;2)
- Tiedtke, M. (1993). Representation of clouds in large-scale models. *Monthly Weather Review*, *121*(11), 3040–3061. [https://doi.org/10.1175/1520-0493\(1993\)121<3040:ROCILS>2.0.CO;2](https://doi.org/10.1175/1520-0493(1993)121<3040:ROCILS>2.0.CO;2)
- Tompkins, A. M., Gierens, K., & Rädcl, G. (2007). Ice supersaturation in the ECMWF integrated forecast system. *Quarterly Journal of the Royal Meteorological Society*, *133*(622), 53–63. <https://doi.org/10.1002/qj.14>
- Vidot, J., Baran, A. J., & Brunel, P. (2015). A new ice cloud parameterization for infrared radiative transfer simulation of cloudy radiances: Evaluation and optimization with IIR observations and ice cloud profile retrieval products. *Journal of Geophysical Research: Atmospheres*, *120*, 6937–6951. <https://doi.org/10.1002/2015JD023462>
- Wu, W., Liu, X., Zhou, D. K., Larar, A. M., Yang, Q., Kizer, S., & Liu, Q. (2017). The application of PCRTM physical retrieval methodology for IASI cloud scene analysis. *IEEE Transactions on Geoscience and Remote Sensing*, *55*(9), 5042–5056. <https://doi.org/10.1109/TGRS.2017.2702006>
- Yang, Q., Liu, X., Yang, P., & Wang, C. (2014). A fast radiative transfer parameterization under cloudy condition in solar spectral region, AGU2014 (A23E-3293).
- Zhou, D., Larar, A., & Liu, X. (2012). Monitoring surface climate with its emissivity derived from satellite measurements, Proc. SPIE 8524, Land Surface Remote Sensing, 85240I (2012/11/21). <https://doi.org/10.1117/12.974215>